

Transverse Josephson diode effect in tilted Dirac systems

W. Zeng*

Department of physics, Jiangsu University, Zhenjiang 212013, China

We theoretically study the transverse charge transport in Josephson junctions based on the tilted Dirac materials with valley-dependent gaps. It is shown that a finite tilt-assisted transverse Josephson Hall current is present under broken time-reversal symmetry. This transverse current is driven by the superconducting phase difference across the junction and exhibits a nonsinusoidal current-phase relation, leading to the transverse Josephson diode effect (TJDE), where the critical currents flow oppositely along the transverse direction are asymmetric. Compared to the conventional longitudinal Josephson diode effect, the predicted TJDE supports a fully polarized diode efficiency with a 100% quality factor and can completely decouple the input signal path from the output, suggesting potential applications for nonreciprocal superconducting devices.

Introduction.—The nonreciprocal charge transport in Josephson junctions manifests as direction-selective critical supercurrents $j_c^+ \neq j_c^-$ with $j_c^{+(-)}$ being the critical supercurrent along the positive (negative) direction of the junction, which is termed as the Josephson diode effect [1–4]. The Josephson diode effect has been observed or proposed in many systems that break both inversion symmetry (IS) and time-reversal symmetry (TRS) [5–9]. The ability of the Josephson diode to conduct current along one direction is characterized by its quality factor [10–12]. Up to now, some highly efficient Josephson diode effects with large quality factors have been reported. The quality factor can be 90% in the Josephson diode effect proposed via asymmetric spin-momentum locking states [13] and can even reach 100% by exploring a simple supercurrent network in the field-free graphene Josephson triode system [14].

However, previous works on the Josephson diode effect focused on the longitudinal direction of the junction, where the output rectified signal is in the direction parallel to the input. A natural question to ask is whether this nonreciprocal diode effect can be generated in the transverse direction of the Josephson junction, so that the paths of the input excitation and the output rectified signal can be decoupled. Recent studies reported that the tilted fermions may induce the transverse transport in tunnel junctions, such as the tunneling valley Hall effect [15], the tunneling chirality Hall effect [16], and the nonlinear valley Hall effect [17], suggesting that the tilted Dirac system serves as a promising platform for designing transverse superconducting devices.

Most of the Dirac materials possess the isotropic spectrum in momentum space, where the Dirac cones are symmetric [18–22]. However, a finite tilt of Dirac cones can occur since the Lorentz symmetry is not necessarily the symmetry group in condensed matter systems [23], such as in the case of strained graphene [24], 8-*Pmmn* borophene [25–27], organic conductor α -(BEDT-TTF)₂I₃ [28], and 1T' monolayer transition metal dichalcogenides [29, 30]. Moreover, a finite valley-dependent band gap can also be generated in the tilted Dirac systems. The

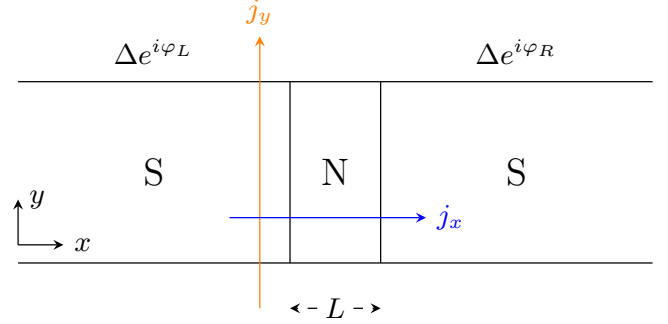


FIG. 1. Schematic illustration of the Josephson junction based on the tilted Dirac material. The longitudinal direction of the junction is along the x axis. The superconducting regions (denoted by S) are located at $x < 0$ and $x > L$, where the s -wave pairing potentials are $\Delta e^{i\varphi_L}$ and $\Delta e^{i\varphi_R}$, respectively. The normal region (N) is located at $0 < x < L$. Both the longitudinal Josephson current j_x and the transverse charge current j_y can be generated.

ab initio calculation suggests that a band opening in 8-*Pmmn* borophene can be achieved by hydrogenation and controlled by strain [31], and the massive fermions in α -(BEDT-TTF)₂I₃ has been experimentally reported [28]. In addition, the off-resonant circularly polarized radiation accompanied by a sublattice staggered potential is also an alternative method for producing the valley-dependent mass in the regime of Floquet picture [32, 33].

In this Letter, we report a study of the transverse transport in the Josephson junctions based on the tilted Dirac materials with valley-dependent gaps. The transverse current is obtained in terms of the Andreev reflection coefficients like the Furusaki-Tsukada formula [34–36], which is analytically derived from the McMillan’s formulation [37, 38]. We find that the finite transverse current appears when the system possesses TRS-broken valley-contrasting gaps. Similar to the conventional longitudinal Josephson current, this transverse current is driven by the superconducting phase difference across the junction and exhibits a nonsinusoidal current-phase rela-

tion, leading to a nonreciprocal transverse transport in the Josephson junction, which allows for a larger critical supercurrent in one transverse direction than in the opposite one. This transverse nonreciprocal transport can be termed as the transverse Josephson diode effect (TJDE). The nonreciprocity is present only in the transverse direction and absent in the longitudinal one with a high TJDE efficiency even reaching up to 100%, which completely decouples the path of the input signal from that of the output one and suggests potential applications for nonreciprocal superconducting devices. We further analyse the discrete Andreev levels confined in the Josephson junction, which can aid in better understanding the TJDE. It is shown that, as a consequence of the tilted Dirac cones, a pair of asymmetric transverse subgap propagating modes appear for each valley under the broken TRS, which is responsible for the transverse current.

Model and formalism.—The Josephson junction under consideration is shown in Fig. 1, where the longitudinal direction of the junction is along the x axis and the superconducting regions are located at $x < 0$ and $x > L$ with L being the length of the junction. The charge carriers in the vicinity of the Dirac points of the anisotropic tilted Dirac systems are described by the Hamiltonian [32, 33, 39, 40]

$$\mathcal{H}_\ell = -i\ell\hbar v_x \partial_x \sigma_x - i\hbar v_y \partial_y \sigma_y - i\ell\hbar v_t \partial_y \sigma_0 + \lambda_\ell \sigma_z, \quad (1)$$

where $\ell = \pm$ labels K and K' valleys, respectively, σ is the Pauli matrix acting on the pseudospin space, (v_x, v_y) and v_t are the direction-dependent velocities and the tilt velocity, respectively. For different valleys, the Dirac cones are tilted in opposite y directions in the momentum space with the same tilt parameter v_t . The valley-dependent mass λ_ℓ is also considered in the normal region of the Josephson junction. Broken TRS leads to the valley-contrasting mass $\lambda_+ \neq \lambda_-$, which is responsible for many peculiar phenomena, such as the intriguing optical properties of tilted Dirac systems [32] and the valley Seebeck effect [33]. In the superconducting regions, the BCS superconductivity can be induced by the conventional superconductor via the proximity effect [41–43], where the paired electrons are from two different valleys. The Bogoliubov-de Gennes (BdG) Hamiltonian describing the quasiparticles in the Josephson junction can be decoupled into two valley sectors [20, 44, 45]. For the ℓ valley sector, the BdG Hamiltonian reads

$$\mathcal{H}_{BdG}^\ell = \begin{pmatrix} \mathcal{H}_\ell - \mu(x) & \Delta(x) \\ \Delta^\dagger(x) & \mu(x) - \mathcal{H}_\ell^* \end{pmatrix}, \quad (2)$$

where the Nambu basis is $(\psi_\ell, \psi_\ell^\dagger)^T$ with ψ_ℓ being the two-component spinors in the sublattice space and $\bar{\ell} = -\ell$. The chemical potential $\mu(x)$ is taken as μ in the normal region and μ_s in the superconducting regions. The pairing potential $\Delta(x)$ is $\Delta e^{i\varphi_L}$ and $\Delta e^{i\varphi_R}$ for left and

right superconducting regions, respectively, with Δ being the amplitude of the pairing potential, φ_L and φ_R being the corresponding superconducting phases.

In order to obtain the transverse current, we first need the expression for the current operator, which can be derived from the continuity equation. The charge density operator $\hat{\rho} = -e \sum_\ell \psi_\ell^\dagger \psi_\ell$ obeys the Heisenberg equation of motion $\partial_t \hat{\rho} = [\hat{\rho}, \mathcal{H}_{BdG}]/i\hbar = -\nabla \cdot \hat{\mathbf{j}}_e - \nabla \cdot \hat{\mathbf{j}}_s$, where \mathcal{H}_{BdG} is the whole BdG Hamiltonian containing both the K and K' valley sectors in Eq. (2), $\hat{\mathbf{j}}_e$ and $\hat{\mathbf{j}}_s$ are the electronic and source current density operators, respectively. The transverse current operator is obtained after completing the calculation of the commutator, which reads $\hat{j}_y = -e \sum_\ell (v_y \psi_\ell^\dagger \sigma_y \psi_\ell + \ell v_t \psi_\ell^\dagger \psi_\ell)$. The total current density is given by $\mathbf{j} = \langle \hat{\mathbf{j}}_e \rangle + \langle \hat{\mathbf{j}}_s \rangle$, whereas the transverse current is only contributed by the electronic term [46] and can be written as $j_y = \sum_\ell j_y^\ell$. Here j_y^ℓ is the transverse current density for ℓ valley and can be expressed in terms of the Matsubara Green's function:

$$j_y^\ell = -\frac{e}{2\beta} \sum_{k_y, \omega_n} \left(v_y \text{tr}[\nu_0 \sigma_y G_\ell] + \ell v_t \text{tr}[\nu_0 \sigma_0 G_\ell] \right), \quad (3)$$

where β is the inverse temperature, $G_\ell = (i\omega_n - H_{BdG}^\ell)^{-1}$ is the Matsubara Green's function for the ℓ sector of the BdG Hamiltonian in Eq. (2) with $\omega_n = (2n + 1)\pi/\beta$, ($n = 0, \pm 1, \pm 2, \dots$) and can be obtained by the analytical continuation from the retarded Green's function G_ℓ^R .

We follow the McMillan's approach [34, 37, 38] for constructing the retarded Green's function G_ℓ^R ; see Supplemental Material. Because of the translational invariance along the y direction, the retarded Green's function can be written as $G_\ell^R(\mathbf{r}, \mathbf{r}') = G_\ell^R(x, x') e^{ik_y(y-y')}$ with k_y being the conserved transverse wave number and

$$G_\ell^R(x, x') = \varrho \times \begin{cases} \Xi_1^\ell / \cos \theta_1 - \Xi_2^\ell / \cos \theta_2, & x > x' \\ \Xi_1^\ell / \cos \theta_1 - \tilde{\Xi}_2^\ell / \cos \theta_2, & x < x', \end{cases} \quad (4)$$

where $\varrho = -iv_x^{-1}\Omega/(E + \Omega)$, $\Omega = \sqrt{E^2 - \Delta^2}$ for $E > \Delta$ and $\Omega = i\sqrt{\Delta^2 - E^2}$ for $E < \Delta$ with E being the energy measured from the Fermi level. $\Xi_{1,2}^\ell$ and $\tilde{\Xi}_{1,2}^\ell$ are matrices constructed by the scattering basis spinors of H_{BdG}^ℓ with $\theta_{1,2}$ being the corresponding transmission angles, which are provided in Supplemental Material. The Matsubara Green's function can be obtained by the analytic continuation $E + i0^+ \rightarrow i\omega_n$ from the retarded Green's function in Eq. (4). We consider the short junction $L \ll \xi_0$, where $\xi_0 = \hbar v_F/\Delta$ is the superconducting coherence length. Without loss of generality, we assume $\varphi_L = 0$ and $\varphi_R = \varphi$ in our model and set $\hbar = 1$ throughout our calculation. The mean-field treatment of superconductivity requires the heavy-doping limit in the superconducting regions, *i.e.*, $|\mu_s| \gg \{|\mu|, \Delta\}$ [20, 44]. In this regime, the transverse current density is expressed

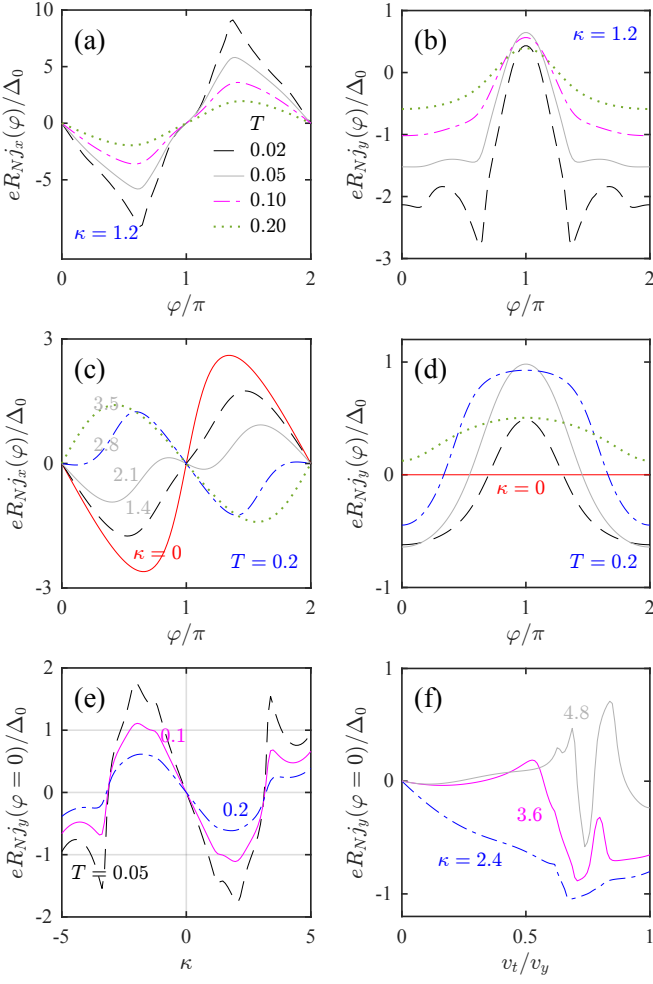


FIG. 2. [(a), (b)] Current-phase relation for $j_x(\varphi)$ and $j_y(\varphi)$ at $\kappa = 1.2$. [(c), (d)] Current-phase relation for $j_x(\varphi)$ and $j_y(\varphi)$ at $T = 0.2$ (in units of T_c). (e) Transverse current at zero phase difference [$j_y(\varphi = 0)$] as a function of κ . (f) $j_y(\varphi = 0)$ as a function of the tilt parameter v_t . The other parameters are $\mu_s = 200\Delta_0$ and $\mu L/\hbar v_F = 4.2$. We normalize the current to $eR_N j_{x,y}/\Delta_0$ with R_N being the resistivity of the junction in normal state.

by the Andreev reflection coefficients

$$j_y^\ell = ek_B T \sum_{k_y, \omega_n} \frac{\Delta}{\sqrt{\omega_n^2 + \Delta^2}} \times \frac{v_y \tan \theta + \ell v_t \sec \theta}{v_x} \times \Re \left(a_1^\ell(\varphi, i\omega_n) + a_2^\ell(\varphi, i\omega_n) \right) e^{2\Omega_n x/v_x}, \quad (5)$$

where k_B is the Boltzmann constant, T is the temperature, $\theta = \arctan(v_y k_y/\mu_s)$, $\Omega_n = \sqrt{\omega_n^2 + \Delta^2}$, $a_1^\ell(\varphi, i\omega_n)$ and $a_2^\ell(\varphi, i\omega_n)$ are the Andreev reflection amplitudes for the electron-like quasiparticles and hole-like quasiparticles, respectively. The longitudinal current (Josephson current) is given by $j_x = \sum_\ell j_x^\ell$, where j_x^ℓ is obtained

from the Furusaki-Tsukada formula [34–36]

$$j_x^\ell = ek_B T \sum_{k_y, \omega_n} \frac{\Delta}{\sqrt{\omega_n^2 + \Delta^2}} \left(a_1^\ell(\varphi, i\omega_n) - a_2^\ell(\varphi, i\omega_n) \right). \quad (6)$$

Transverse Josephson diode effect.—We consider the parameters $v_x = 0.86v_F$, $v_y = 0.69v_F$, and $v_t = 0.32v_F$ corresponding to the two-dimensional material 8-*Pmmn* borophene [26, 47–49], where $v_F = 10^6$ m/s. The temperature dependence of the pairing potential is assumed to be $\Delta(T) = \Delta_0 \tanh(1.74\sqrt{T_c/T - 1})$ with $\Delta_0 = 1.76k_B T_c$, where T_c is the critical temperature. We define a dimensionless parameter, $\kappa = (\lambda_+ - \lambda_-)/\Delta_0$, to represent the discrepancy between the two valley-dependent gaps.

The current-phase relation (CPR) of the longitudinal Josephson current density $j_x(\varphi)$ is shown in Fig. 2(a) at $\kappa = 1.2$. $j_x(\varphi)$ exhibits a sinusoidal π -phase CPR. The critical current of $j_x(\varphi)$ decreases with the increasing of the temperature T , but the CPR remains a π phase. $j_x(\varphi)$ at $T = 0.2$ (in units of T_c) for different κ is shown in Fig. 2(c). The Josephson current changes its sign and the 0 - π phase transition occurs with the increasing of κ . Similar to the 0 - π transition in SFS Josephson junctions [50, 51] (F represents the ferromagnetic metal), the supercurrent reversal is attributed to the valley polarization induced by the broken TRS, where the valley-singlet Cooper pairs acquire a nonzero momentum [52]. The Josephson current holds the relation $j_x(\varphi) = -j_x(-\varphi)$ for both 0 - and π -phase CPRs. Consequently, the anomalous supercurrent flowing at zero phase difference is absent. The forward and backward critical currents are symmetric, *i.e.*, $j_x^+ = j_x^-$, which indicates the absence of the diode effect in the longitudinal direction.

The transverse current has its maximum value at the NS boundary and decays exponentially into the S region, we present the CPRs of the transverse current at the NS interface ($x = 0$) in Figs. 2(b) and 2(d). The critical current of $j_y(\varphi)$ decreases with the increasing of T ; see Fig. 2(b). Distinct from the longitudinal Josephson current, $j_y(\varphi)$ disappears at $\kappa = 0$ where the TRS is preserved, as shown in Fig. 2(d). However, a finite transverse current flows even at zero phase difference. This anomalous transverse current $j_y(\varphi = 0)$ exhibits a symmetric relation of κ [$j_y(\varphi = 0, \kappa) = -j_y(\varphi = 0, -\kappa)$] and can be further enhanced by either decreasing the temperature or tilting the Dirac cones; see Figs. 2(e) and 2(f).

Analogous to the Hall angle of the conventional tunneling Hall effect in tunnel junctions [15, 16, 53, 54], the efficiency of the conversion of the longitudinal and transverse current in the Josephson junction is in proportion to j_y/j_x , reaching its maximum value at $\varphi = n\pi$, ($n \in \mathbb{Z}$), where a pure transverse current is present without the longitudinal Josephson current. There is a subtle difference between the predicted Josephson Hall effect in our

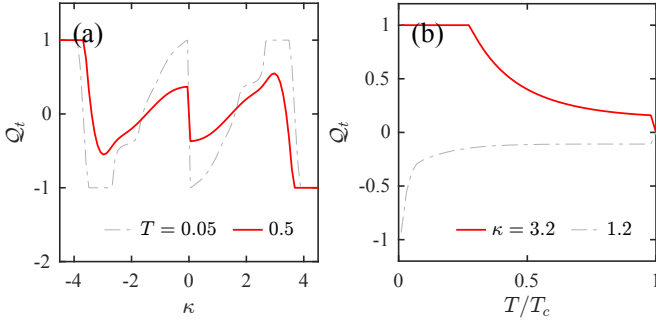


FIG. 3. (a) Quality factor of the TJDE Q_t as a function of κ . (b) Quality factor versus the temperature T .

model and the previously proposed tunneling Hall effect in the tunnel junctions based on the tilted Dirac materials. The latter effect is associated with the momentum filtering due to the mismatch of the tilted Fermi surfaces in different regions of the heterojunctions [15, 16], where the electron tunneling is skewed. However, we will point out that this skew-tunneling mechanism plays a minor role in the Josephson Hall effect. The transverse current in Eq. (3) can be decomposed into two parts: $j_y^\ell = j_{y,1}^\ell + j_{y,2}^\ell$ with $j_{y,1}^\ell \sim (v_y/v_x) \sum_{j=1,2} \int_{-\pi/2}^{\pi/2} d\theta a_j^\ell(\theta) \tan \theta$ and $j_{y,2}^\ell \sim (v_t/v_x) \sum_{j=1,2} \int_{-\pi/2}^{\pi/2} d\theta \ell a_j^\ell(\theta) / \cos \theta$, where we replace the summation over k_y by the integration over θ . $j_{y,1}^\ell$ is related to the skew-tunneling and is absent when the scattering is symmetric, *i.e.*, $a_j^\ell(\theta) = a_j^\ell(-\theta)$, whereas $j_{y,2}^\ell$ is attributed to the tilt-induced nonzero transverse momentum acquired by the quasiparticles. In the heavy-doping regime, $j_{y,1}^\ell$ is much smaller than $j_{y,2}^\ell$ with the scale $j_{y,1}^\ell/j_{y,2}^\ell \sim |\mu/\mu_s|$. As a result, $j_{y,2}^\ell$ is dominant in the proposed Josephson Hall effect, where the transverse current is driven by the passage of the Cooper pair across the junction carrying a finite tilt-induced transverse momentum.

Most notably, $j_y(\varphi)$ is a periodic function of φ with a period of 2π but possesses a nonsinusoidal CPR, which indicates a nonreciprocal transverse charge transport in the Josephson junction. The extent of the nonreciprocal in the transverse direction of the Josephson junction is characterized by the quality factor:

$$Q_t = \frac{j_{y,c}^+ - |j_{y,c}^-|}{j_{y,c}^+ + |j_{y,c}^-|}, \quad (7)$$

where $j_{y,c}^+$ ($j_{y,c}^-$) is the critical current along the positive (negative) transverse direction of the junction and the sign of Q_t defines the transverse diode polarity. In Fig. 3(a), we present the quality factor of the TJDE as a function of κ . The quality factor exhibits the symmetric relation $Q_t(\kappa) = -Q_t(-\kappa)$. This symmetric behavior of Q_t is similar to that of the longitudinal Josephson diode effect predicted on the surface of topological insulators

[6], where the broken TRS is induced by the external magnetic field. Remarkably, the quality factor can even reach 100% by tuning the valley-dependent band gaps. The temperature-dependence of the transverse quality factor is shown in Fig. 3(b). For both the positive and negative transverse diode polarity [$Q_t > 0$ and $Q_t < 0$, respectively], the TJDE efficiency at low temperature is generally greater than that at high temperature.

Although the transverse current obtained in Eq. (5) includes contributions from both the discrete and continuum spectra, the TJDE can be qualitatively understood in terms of the Andreev bound states (ABSs) confined in the normal region, which arise from the closed-loop motion of the carriers with discrete subgap energies. For $E < \Delta$, there are no propagating modes in the superconducting regions. We can then define the transfer matrix for the Andreev reflection at the NS interfaces, which is given by $\mathcal{S}_{+(-)} = e^{-i\varphi_{R(L)} - (+)i\ell\alpha\sigma_x}$ with $\alpha = \arccos(E/\Delta)$ for the right (left) interface [55, 56]. The transfer matrix for the carriers in the normal region can be obtained by the direct integration of the BdG equation [57, 58], which yields $\psi(x) = e^{\int_{x_0}^x i\ell v_x^{-1} v_z \sigma_x \mathcal{O} dx'} \psi(x_0)$ with $\mathcal{O} = E \times \mathbb{1} - \mathcal{H}_{BdG}^\ell|_{k_x=0}$. The electron and hole states are decoupled in the normal region due to the absence of the superconductivity. As a result, \mathcal{O} is a block diagonal matrix. Evaluating the integral across the normal region gives rise to

$$e^{i\ell L v_z \sigma_x \mathcal{O} / v_x} = \begin{pmatrix} \mathcal{M} & \emptyset \\ \emptyset & \mathcal{M}' \end{pmatrix}, \quad (8)$$

where \mathcal{M} and \mathcal{M}' are the transfer matrices for the electron and hole states, respectively. For the existence of ABSs in the Josephson junction, the Andreev process between two NS interfaces forms a closed loop and the transfer matrix $\mathcal{M}^{-1} \mathcal{S}_+^{-1} \mathcal{M}' \mathcal{S}_-$ is unimodular, which in turn gives the discrete Andreev levels E_{ABS} .

The numerical results of the transverse-momentum-dependence of E_{ABS} are presented in Fig. 4. When the tilt is absent ($v_t = 0$), the ABS energy levels are symmetric with respect to the transverse momentum, *i.e.*, $E_{ABS}(k_y, \varphi) = E_{ABS}(-k_y, \varphi)$; see Fig. 4(a). For each transverse propagating mode at $|+k_y\rangle$ with the group velocity $v(k_y) = \partial E_{ABS}(k_y, \varphi) / \partial k_y$, there always exists an oppositely propagating mode at $|-k_y\rangle$ with its group velocity being $-v(k_y)$. Consequently, the transverse current is always absent.

For the TRS-preserved tilted Dirac systems ($\kappa = 0$ and $v_t \neq 0$), the ABS spectra are skewed to opposite k_y directions for the opposite valleys due to the tilt of the Dirac cones; see Fig. 4(b). However, E_{ABS} is symmetric with respect to $E = 0$ due to TRS, which holds the relation $E_{ABS}(k_y, \varphi) = -E_{ABS}(k_y, \varphi)$. For each transverse propagating mode with group velocity v_+ , there always exists an oppositely propagating mode at the same transverse momentum with group velocity v_- , where $v_+ = -v_-$. Thus, the transverse current is also absent.

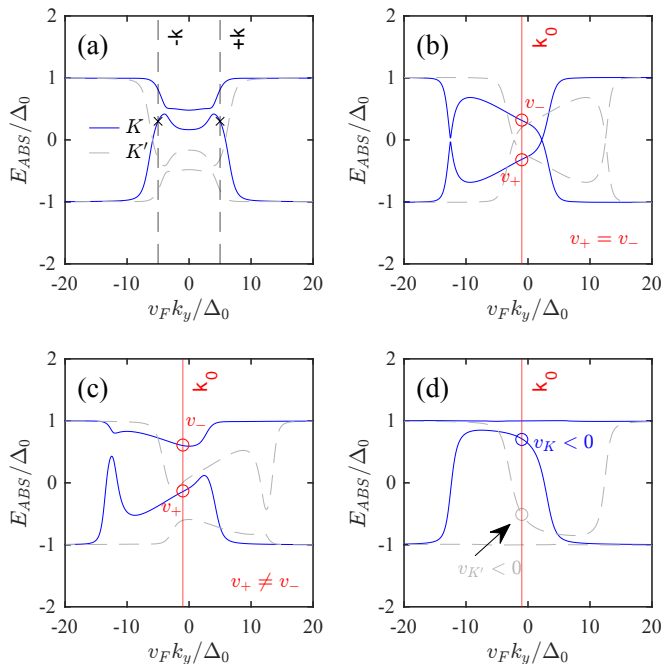


FIG. 4. Andreev level E_{ABS} versus the transverse wave number k_y at $T = 0$ K. The blue solid lines and the gray dashed lines denote the E_{ABS} for K and K' valleys, respectively. (a) $v_t = 0$ and $\kappa = 1.2$. (b) $v_t = 0.32v_F$ and $\kappa = 0$. [(c), (d)] $v_t = 0.32v_F$, $\kappa = 1.2$ and 1.6 for (c) and (d), respectively. The other parameters are $\varphi_L = 0$, $\varphi_R = \pi$, and $\mu_s = 200\Delta_0$.

The ABS energy levels of the broken-TRS tilted Dirac systems are shown in Figs. 4(c) and 4(d). We focus on the small k_y regime, which makes a dominant contribution in Josephson effects. For a given valley, there are two subgap transverse modes propagating in the opposite y directions at $\kappa = 1.2$, with their group velocities being v_+ and v_- , respectively; see Fig. 4(c). The transverse nonreciprocal transport is generated as a consequence of $v_+ \neq v_-$. For $\kappa = 1.6$, only one propagating subgap mode appears for each valley; see Fig. 4(d). In the small k_y regime, both the subgap modes from K and K' valley are propagating along the negative transverse direction with their group velocities being $v_{K,K'} < 0$. The positive propagating modes are absent. Distinct from the conventional Josephson diode effect along the longitudinal direction, the predicted TJDE is attributed to the tilt-induced asymmetric transverse propagating modes, rather than the Doppler shift of the quasiparticle energies [13, 59, 60].

Conclusions.—To conclude, we study the transverse charge transport in the Josephson junctions based on the tilted Dirac materials with valley-dependent gaps. The transverse charge current is expressed by Andreev reflection coefficients like the Furusaki-Tsukada formula, which is theoretically obtained by using the McMillan's Green's function. It is shown that the tilt-assisted transverse cur-

rent can be generated under broken TRS and is driven by the superconducting phase difference across the junction. The transverse critical current is direction-selective, resulting in a nonreciprocal transverse transport, namely, the transverse Josephson diode effect. The nonreciprocity is present only in the transverse direction and absent in the longitudinal one with a high TJDE efficiency even reaching up to 100%, which completely decouples the path of the input signal from that of the output one and suggests potential applications for nonreciprocal superconducting devices.

Acknowledgements.—I wish gratefully to acknowledge discussions with Professor Bo Lu (Tianjin University) and Professor Wei Chen (Nanjing University).

* E-mail: zeng@ujts.edu.cn

- [1] Y. Zhang, Y. Gu, P. Li, J. Hu, and K. Jiang, General theory of Josephson diodes, *Phys. Rev. X* **12**, 041013 (2022).
- [2] J. Hu, C. Wu, and X. Dai, Proposed design of a Josephson diode, *Phys. Rev. Lett.* **99**, 067004 (2007).
- [3] Z. Liu, L. Huang, and J. Wang, Josephson diode effect in topological superconductors, *Phys. Rev. B* **110**, 014519 (2024).
- [4] J.-X. Hu, Z.-T. Sun, Y.-M. Xie, and K. T. Law, Josephson diode effect induced by valley polarization in twisted bilayer graphene, *Phys. Rev. Lett.* **130**, 266003 (2023).
- [5] R. S. Souto, M. Leijnse, and C. Schrade, Josephson diode effect in supercurrent interferometers, *Phys. Rev. Lett.* **129**, 267702 (2022).
- [6] B. Lu, S. Ikegaya, P. Buset, Y. Tanaka, and N. Nagaosa, Tunable Josephson diode effect on the surface of topological insulators, *Phys. Rev. Lett.* **131**, 096001 (2023).
- [7] J. Wang, Y. Jiang, J. J. Wang, and J.-F. Liu, Efficient Josephson diode effect on a two-dimensional topological insulator with asymmetric magnetization, *Phys. Rev. B* **109**, 075412 (2024).
- [8] A. Costa, J. Fabian, and D. Kochan, Microscopic study of the Josephson supercurrent diode effect in Josephson junctions based on two-dimensional electron gas, *Phys. Rev. B* **108**, 054522 (2023).
- [9] J. Cayao, N. Nagaosa, and Y. Tanaka, Enhancing the Josephson diode effect with Majorana bound states, *Phys. Rev. B* **109**, L081405 (2024).
- [10] P. A. Volkov, E. Lantagne-Hurtubise, T. Tummuru, S. Plugge, J. H. Pixley, and M. Franz, Josephson diode effects in twisted nodal superconductors, *Phys. Rev. B* **109**, 094518 (2024).
- [11] B. Scharf, D. Kochan, and A. Matos-Abiague, Superconducting diode effect in quantum spin Hall insulator based Josephson junctions, *Phys. Rev. B* **110**, 134511 (2024).
- [12] Y. Tanaka, B. Lu, and N. Nagaosa, Theory of giant diode effect in d -wave superconductor junctions on the surface of a topological insulator, *Phys. Rev. B* **106**, 214524 (2022).
- [13] P.-H. Fu, Y. Xu, S. A. Yang, C. H. Lee, Y. S. Ang, and J.-F. Liu, Field-effect Josephson diode via asymmetric spin-momentum locking states, *Phys. Rev. Appl.* **21**, 054057 (2024).

- (2024).
- [14] J. Chiles, E. G. Arnault, C.-C. Chen, T. F. Larson, L. Zhao, K. Watanabe, T. Taniguchi, F. Amet, and G. Finkelstein, Nonreciprocal supercurrents in a field-free graphene Josephson triode, *Nano Letters* **23**, 5257 (2023).
- [15] S.-H. Zhang, D.-F. Shao, Z.-A. Wang, J. Yang, W. Yang, and E. Y. Tsymbal, Tunneling valley Hall effect driven by tilted Dirac fermions, *Phys. Rev. Lett.* **131**, 246301 (2023).
- [16] W. Zeng, Tunneling chirality Hall effect in type-I Weyl semimetals, *Phys. Rev. B* **110**, 024511 (2024).
- [17] K. Das, K. Ghorai, D. Culcer, and A. Agarwal, Nonlinear valley Hall effect, *Phys. Rev. Lett.* **132**, 096302 (2024).
- [18] A. Avsar, H. Ochoa, F. Guinea, B. Özyilmaz, B. J. van Wees, and I. J. Vera-Marun, Colloquium: Spintronics in graphene and other two-dimensional materials, *Rev. Mod. Phys.* **92**, 021003 (2020).
- [19] N. P. Armitage, E. J. Mele, and A. Vishwanath, Weyl and Dirac semimetals in three-dimensional solids, *Rev. Mod. Phys.* **90**, 015001 (2018).
- [20] C. W. J. Beenakker, Specular Andreev reflection in graphene, *Phys. Rev. Lett.* **97**, 067007 (2006).
- [21] W. Zeng and R. Shen, Andreev reflection of massive pseudospin-1 fermions, *New Journal of Physics* **24**, 043021 (2022).
- [22] Y. Huang, W. Zeng, and R. Shen, Photoinduced Klein tunneling in semi-Dirac material, *Physics Letters A* **463**, 128671 (2023).
- [23] S. A. Jafari, Electric field assisted amplification of magnetic fields in tilted Dirac cone systems, *Phys. Rev. B* **100**, 045144 (2019).
- [24] M. O. Goerbig, J.-N. Fuchs, G. Montambaux, and F. Piéchon, Tilted anisotropic Dirac cones in quinoid-type graphene and α -(BEDT-TTF)₂I₃, *Phys. Rev. B* **78**, 045415 (2008).
- [25] X.-F. Zhou, X. Dong, A. R. Oganov, Q. Zhu, Y. Tian, and H.-T. Wang, Semimetallic two-dimensional boron allotrope with massless Dirac fermions, *Phys. Rev. Lett.* **112**, 085502 (2014).
- [26] A. Lopez-Bezanilla and P. B. Littlewood, Electronic properties of 8-*Pmmn* borophene, *Phys. Rev. B* **93**, 241405 (2016).
- [27] M. Nakhaee, S. A. Ketabi, and F. M. Peeters, Tight-binding model for borophene and borophane, *Phys. Rev. B* **97**, 125424 (2018).
- [28] S. Katayama, A. Kobayashi, and Y. Suzumura, Pressure-induced zero-gap semiconducting state in organic conductor α -(BEDT-TTF)₂I₃ salt, *Journal of the Physical Society of Japan* **75**, 054705 (2006).
- [29] C.-Y. Tan, C.-X. Yan, Y.-H. Zhao, H. Guo, and H.-R. Chang, Anisotropic longitudinal optical conductivities of tilted Dirac bands in 1T'-MoS₂, *Phys. Rev. B* **103**, 125425 (2021).
- [30] X. Qian, J. Liu, L. Fu, and J. Li, Quantum spin Hall effect in two-dimensional transition metal dichalcogenides, *Science* **346**, 1344 (2014).
- [31] Z.-Q. Wang, T.-Y. Lü, H.-Q. Wang, Y. P. Feng, and J.-C. Zheng, Band gap opening in 8-*Pmmn* borophene by hydrogenation, *ACS Applied Electronic Materials* **1**, 667 (2019).
- [32] M. A. Mojarro, R. Carrillo-Bastos, and J. A. Maytorena, Optical properties of massive anisotropic tilted Dirac systems, *Phys. Rev. B* **103**, 165415 (2021).
- [33] P. Kapri, B. Dey, and T. K. Ghosh, Valley caloritronics in a photodriven heterojunction of Dirac materials, *Phys. Rev. B* **102**, 045417 (2020).
- [34] A. Furusaki and M. Tsukada, Dc Josephson effect and Andreev reflection, *Solid State Communications* **78**, 299 (1991).
- [35] Y. Zhao and R. Shen, Josephson effect in junctions of ferromagnetic superconductors with equal spin pairing symmetry, *Phys. Rev. B* **73**, 214511 (2006).
- [36] B. Lu, K. Maeda, H. Ito, K. Yada, and Y. Tanaka, φ Josephson junction induced by altermagnetism, *Phys. Rev. Lett.* **133**, 226002 (2024).
- [37] W. L. McMillan, Theory of superconductor—normal-metal interfaces, *Phys. Rev.* **175**, 559 (1968).
- [38] Y. Tanaka and S. Kashiwaya, Theory of Josephson effects in anisotropic superconductors, *Phys. Rev. B* **56**, 892 (1997).
- [39] M. A. Mojarro, R. Carrillo-Bastos, and J. A. Maytorena, Hyperbolic plasmons in massive tilted two-dimensional Dirac materials, *Phys. Rev. B* **105**, L201408 (2022).
- [40] C.-Y. Tan, J.-T. Hou, C.-X. Yan, H. Guo, and H.-R. Chang, Signatures of Lifshitz transition in the optical conductivity of two-dimensional tilted Dirac materials, *Phys. Rev. B* **106**, 165404 (2022).
- [41] M. Ben Shalom, M. Zhu, V. Fal'ko, A. Mishchenko, A. Kretinin, K. Novoselov, C. Woods, K. Watanabe, T. Taniguchi, A. Geim, *et al.*, Quantum oscillations of the critical current and high-field superconducting proximity in ballistic graphene, *Nature Physics* **12**, 318 (2016).
- [42] P. Buset, A. L. Yeyati, and A. Martín-Rodero, Microscopic theory of the proximity effect in superconductor-graphene nanostructures, *Phys. Rev. B* **77**, 205425 (2008).
- [43] U. C. Coskun, M. Brenner, T. Hymel, V. Vakaryuk, A. Levchenko, and A. Bezryadin, Distribution of supercurrent switching in graphene under the proximity effect, *Phys. Rev. Lett.* **108**, 097003 (2012).
- [44] C. W. J. Beenakker, Colloquium: Andreev reflection and Klein tunneling in graphene, *Rev. Mod. Phys.* **80**, 1337 (2008).
- [45] P.-G. De Gennes, *Superconductivity of metals and alloys* (CRC press, 2018).
- [46] P. M. R. Brydon, C. Timm, and A. P. Schnyder, Interface currents in topological superconductor-ferromagnet heterostructures, *New Journal of Physics* **15**, 045019 (2013).
- [47] G. C. Paul, S. F. Islam, and A. Saha, Fingerprints of tilted Dirac cones on the RKKY exchange interaction in 8-*Pmmn* borophene, *Phys. Rev. B* **99**, 155418 (2019).
- [48] E. Vanderstraeten and D. Vande Ginste, Valley filtering in 8-*Pmmn* borophene based on an electrostatic waveguide constriction, *Phys. Rev. B* **109**, 205413 (2024).
- [49] A. E. Champo and G. G. Naumis, Metal-insulator transition in 8-*pmmn* borophene under normal incidence of electromagnetic radiation, *Phys. Rev. B* **99**, 035415 (2019).
- [50] A. I. Buzdin, A. S. Mel'nikov, and N. G. Pugach, Domain walls and long-range triplet correlations in SFS Josephson junctions, *Phys. Rev. B* **83**, 144515 (2011).
- [51] B. Crouzy, S. Tollis, and D. A. Ivanov, Josephson current in a superconductor-ferromagnet-superconductor junction with in-plane ferromagnetic domains, *Phys. Rev. B* **76**, 134502 (2007).
- [52] J. Wang, Y. H. Yang, and K. S. Chan, Josephson π state

- induced by valley polarization, *Phys. Rev. B* **89**, 064501 (2014).
- [53] A. Matos-Abiague and J. Fabian, Tunneling anomalous and spin Hall effects, *Phys. Rev. Lett.* **115**, 056602 (2015).
- [54] B. Scharf, A. Matos-Abiague, J. E. Han, E. M. Hankiewicz, and I. Žutić, Tunneling planar Hall effect in topological insulators: Spin valves and amplifiers, *Phys. Rev. Lett.* **117**, 166806 (2016).
- [55] M. Titov and C. W. J. Beenakker, Josephson effect in ballistic graphene, *Phys. Rev. B* **74**, 041401 (2006).
- [56] W. Zeng and R. Shen, Light-modulated Josephson effect in Kekulé patterned graphene, *Phys. Rev. B* **105**, 094510 (2022).
- [57] A. R. Akhmerov and C. W. J. Beenakker, Boundary conditions for Dirac fermions on a terminated honeycomb lattice, *Phys. Rev. B* **77**, 085423 (2008).
- [58] D. M. Basko, Boundary problems for Dirac electrons and edge-assisted Raman scattering in graphene, *Phys. Rev. B* **79**, 205428 (2009).
- [59] M. Davydova, S. Prembabu, and L. Fu, Universal Josephson diode effect, *Science Advances* **8**, eabo0309 (2022).
- [60] A. Daido, Y. Ikeda, and Y. Yanase, Intrinsic superconducting diode effect, *Phys. Rev. Lett.* **128**, 037001 (2022).

Supplementary Material for “Transverse Josephson diode effect in tilted Dirac systems”

W. Zeng*

Department of physics, Jiangsu University, Zhenjiang 212013, China

In this Supplemental Material, we present the calculation for constructing the Green’s function using McMillan’s formulation and provide the detailed derivations of the transverse current in the Josephson junction.

The Green’s function can be constructed by the elementary scattering processes of the BdG Hamiltonian by the McMillan’s formula [1–3]. We set $\hbar = 1$ throughout our calculation. The independent wave functions can be obtained by solving the scattering problem described by the secular equation $[E - H_{BdG}^\ell(\mathbf{r}, \partial_{\mathbf{r}})]\psi(x)e^{ik_y y} = 0$ with k_y being the conversed transverse wave vector and $\ell = \pm$ being the valley index, yielding the scattering states

$$\psi_1(x) = A_1 e^{+ik_1 x} + a_1^\ell A_4 e^{+ik_2 x} + b_1^\ell A_3 e^{-ik_1 x}, \quad (S1)$$

$$\psi_2(x) = A_2 e^{-ik_2 x} + a_2^\ell A_3 e^{-ik_1 x} + b_2^\ell A_4 e^{+ik_2 x}, \quad (S2)$$

$$\psi_3(x) = c_3^\ell A_1 e^{-ik_1 x} + d_3^\ell A_4 e^{+ik_2 x}, \quad (S3)$$

$$\psi_4(x) = c_4^\ell A_4 e^{+ik_2 x} + d_4^\ell A_3 e^{-ik_1 x}, \quad (S4)$$

where $a^\ell, b^\ell, c^\ell, d^\ell$ are the scattering amplitudes. The basis spinors for the right-propagating electron-like quasiparticles (ELQ) and hole-like quasiparticles (HLQ) are given by

$$A_1 = \begin{pmatrix} 1 \\ \ell e^{i\ell\theta_1} \\ \ell\gamma \\ e^{i\ell\theta_1}\gamma \end{pmatrix}, \quad A_2 = \begin{pmatrix} -\ell e^{i\ell\theta_2}\gamma \\ \gamma \\ -e^{i\ell\theta_2} \\ \ell \end{pmatrix}, \quad (S5)$$

respectively, whereas the basis spinors for the left-propagating ELQ and HLQ are given by

$$A_3 = \begin{pmatrix} -\ell e^{i\ell\theta_1} \\ 1 \\ -e^{i\ell\theta_1}\gamma \\ \ell\gamma \end{pmatrix}, \quad A_4 = \begin{pmatrix} \gamma \\ \ell e^{i\ell\theta_2}\gamma \\ \ell \\ e^{i\ell\theta_2} \end{pmatrix}, \quad (S6)$$

where $\gamma = \Delta/(E + \Omega)$ with $\Omega = \sqrt{E^2 - \Delta^2}$ for $E > \Delta$ and $\Omega = i\sqrt{\Delta^2 - E^2}$ for $E < \Delta$. The angle parameter is given by $\theta_{1,(2)} = \arctan(v_y k_y / v_x k_{1,(2)})$ with $k_{1,(2)}$ being the longitudinal wave vector for ELQ (HLQ), which is given by

$$k_{1,(2)} = v_x^{-1} \sqrt{(\mu_s - \ell v_t k_y + (-)\Omega)^2 - (v_y k_y)^2}. \quad (S7)$$

The conjugate Hamiltonian is given by $\tilde{H}_{BdG}^\ell(\mathbf{r}, \partial_{\mathbf{r}}) = [H_{BdG}^\ell(\mathbf{r}, -\partial_{\mathbf{r}})]^T$, and the corresponding conjugate scattering states are governed by the secular equation $[E - \tilde{H}_{BdG}^\ell(\mathbf{r}', \partial_{\mathbf{r}'})]\tilde{\psi}(x')e^{-ik_y y'} = 0$, resulting in

$$\tilde{\psi}_1(x') = B_1 e^{+ik_1 x'} + \tilde{a}_1^\ell B_4 e^{+ik_2 x'} + \tilde{b}_1^\ell B_3 e^{-ik_1 x'}, \quad (S8)$$

$$\tilde{\psi}_2(x') = B_2 e^{-ik_2 x'} + \tilde{a}_2^\ell B_3 e^{-ik_1 x'} + \tilde{b}_2^\ell B_4 e^{+ik_2 x'}, \quad (S9)$$

$$\tilde{\psi}_3(x') = \tilde{c}_3^\ell B_1 e^{-ik_1 x'} + \tilde{d}_3^\ell B_4 e^{+ik_2 x'}, \quad (S10)$$

$$\tilde{\psi}_4(x') = \tilde{c}_4^\ell B_4 e^{+ik_2 x'} + \tilde{d}_4^\ell B_3 e^{-ik_1 x'}, \quad (S11)$$

where $\tilde{a}^\ell, \tilde{b}^\ell, \tilde{c}^\ell, \tilde{d}^\ell$ and B_i ($i = 1, 2, 3, 4$) are the counterparts of $a^\ell, b^\ell, c^\ell, d^\ell$ and A_i , respectively. The scattering basis spinors (B_i) are given by

$$B_1 = \begin{pmatrix} \ell e^{-i\ell\theta_1} \\ -1 \\ \gamma e^{-i\ell\theta_1} \\ \ell\gamma \end{pmatrix}, \quad B_2 = \begin{pmatrix} \gamma \\ \ell\gamma e^{-i\ell\theta_2} \\ \ell \\ e^{-i\ell\theta_2} \end{pmatrix}, \quad B_3 = \begin{pmatrix} 1 \\ \ell e^{-i\ell\theta_1} \\ \ell\gamma \\ \gamma e^{-i\ell\theta_1} \end{pmatrix}, \quad B_4 = \begin{pmatrix} \ell\gamma e^{-i\ell\theta_2} \\ -\gamma \\ e^{-i\ell\theta_2} \\ -\ell \end{pmatrix}. \quad (S12)$$

The retarded Green's function can be constructed by the scattering states obtained in Eqs. (S1)-(S4) and (S8)-(S11). We present the result for the left superconducting region ($x < 0$). Due to the translational symmetry parallel to the junction, the retarded Green's function reads $G_\ell^R(x, x', y, y') = G_\ell^R(x, x')e^{ik_y(y-y')}$, where [3]

$$G_\ell^R(x, x') = \begin{cases} \alpha_1\psi_1(x)\tilde{\psi}_3^T(x') + \alpha_2\psi_1(x)\tilde{\psi}_4^T(x') + \alpha_3\psi_2(x)\tilde{\psi}_3^T(x') + \alpha_4\psi_2(x)\tilde{\psi}_4^T(x'), & x > x', \\ \beta_1\psi_3(x)\tilde{\psi}_1^T(x') + \beta_2\psi_4(x)\tilde{\psi}_1^T(x') + \beta_3\psi_3(x)\tilde{\psi}_2^T(x') + \beta_4\psi_4(x)\tilde{\psi}_2^T(x'), & x < x'. \end{cases} \quad (\text{S13})$$

The Green's function satisfies the following boundary condition obtained by integrating the BdG equation at $x = x'$,

$$G_\ell^R(x + 0^+, x) - G_\ell^R(x + 0^-, x) = -iv_x^{-1}\ell v_z \sigma_x, \quad (\text{S14})$$

which leads to the detailed balanced relations $a_1^\ell/\cos\theta_1 = -\tilde{a}_2^\ell/\cos\theta_2$, $\tilde{a}_1^\ell/\cos\theta_1 = -a_2^\ell/\cos\theta_2$, $b_{1,2}^\ell = \tilde{b}_{1,2}^\ell$, and the following identities

$$\alpha_1\tilde{c}_3^\ell + \alpha_2\tilde{d}_4^\ell = \beta_1c_3^\ell + \beta_2d_4^\ell = \frac{-i}{2v_x(1-\gamma^2)\cos\theta_1}, \quad (\text{S15})$$

$$\alpha_3\tilde{d}_3^\ell + \alpha_4\tilde{c}_4^\ell = \beta_3d_3^\ell + \beta_4c_4^\ell = \frac{i}{2v_x(1-\gamma^2)\cos\theta_2}, \quad (\text{S16})$$

$$\alpha_3\tilde{c}_3^\ell + \alpha_4\tilde{d}_4^\ell = \alpha_1\tilde{d}_3^\ell + \alpha_2\tilde{c}_4^\ell = \beta_1d_3^\ell + \beta_2c_4^\ell = \beta_3c_3^\ell + \beta_4d_4^\ell = 0. \quad (\text{S17})$$

Consequently, with the help of Eqs. (S15)-(S17), the solved retarded Green's function is given by

$$G_\ell^R(x, x', E) = \frac{-i}{2v_x(1-\gamma^2)} \times \begin{cases} \Xi_1^\ell/\cos\theta_1 - \Xi_2^\ell/\cos\theta_2 & x > x', \\ \tilde{\Xi}_1^\ell/\cos\theta_1 - \tilde{\Xi}_2^\ell/\cos\theta_2, & x < x', \end{cases} \quad (\text{S18})$$

where

$$\Xi_1^\ell = A_1B_3^T e^{+ik_1(x-x')} + a_1^\ell A_4B_3^T e^{+ik_2x-ik_1x'} + b_1^\ell A_3B_3^T e^{-ik_1(x+x')}, \quad (\text{S19})$$

$$\Xi_2^\ell = A_2B_4^T e^{-ik_2(x-x')} + a_2^\ell A_3B_4^T e^{-ik_1x+ik_2x'} + b_2^\ell A_4B_4^T e^{+ik_2(x+x')}, \quad (\text{S20})$$

$$\tilde{\Xi}_1^\ell = A_3B_1^T e^{-ik_1(x-x')} + \tilde{a}_1^\ell A_3B_4^T e^{-ik_1x+ik_2x'} + \tilde{b}_1^\ell A_3B_3^T e^{-ik_1(x+x')}, \quad (\text{S21})$$

$$\tilde{\Xi}_2^\ell = A_4B_2^T e^{+ik_2(x-x')} + \tilde{a}_2^\ell A_4B_3^T e^{+ik_2x-ik_1x'} + \tilde{b}_2^\ell A_4B_4^T e^{+ik_2(x+x')}. \quad (\text{S22})$$

Substituting $\gamma = \Delta/(E + \Omega)$ into Eq. (S18) gives rise to Eq. (4) in the main text.

With the help of the transverse current operator $\hat{j}_y = \sum_\ell \hat{j}_y^\ell$ with $\hat{j}_y^\ell = -e(v_y\psi_\ell^\dagger\sigma_y\psi_\ell + \ell v_t\psi_\ell^\dagger\psi_\ell)$, the transverse current j_y^ℓ can be expressed in terms of the Matsubara Green's function:

$$j_y^\ell = \langle \hat{j}_y^\ell \rangle = -\frac{e}{2\beta} \sum_{k_y, \omega_n} \left(v_y \text{tr}[\nu_0 \sigma_y G_\ell(\mathbf{r}, \mathbf{r}, i\omega_n)] + \ell v_t \text{tr}[\nu_0 \sigma_0 G_\ell(\mathbf{r}, \mathbf{r}, i\omega_n)] \right). \quad (\text{S23})$$

The Matsubara Green's function for the BdG Hamiltonian \mathcal{H}_{BdG}^ℓ is defined by $G_\ell(\mathbf{r}, \tau; \mathbf{r}', \tau') = -\langle \mathcal{T} \phi_\ell(\mathbf{r}, \tau) \phi_\ell^\dagger(\mathbf{r}', \tau') \rangle$, where \mathcal{T} is the time-ordering operator, $\phi_\ell = (\psi_\ell, \psi_\ell^\dagger)^T$ is the Nambu spinor, and τ (τ') represents the imaginary time.

For the positive frequency $\omega_n > 0$, the Matsubara Green's function can be obtained by the analytic continuation $E + i0^+ \rightarrow i\omega_n$ from the retarded Green's function G_ℓ^R , which has been already obtained by the scattering method. As a result, the expectation values of \hat{j}_y^ℓ are evaluated in terms of the Green's function with the summation over the Matsubara frequency and the wave number along the y direction, which gives rise to the transverse current

$$\langle \hat{j}_y^\ell \rangle_{\omega_n > 0} = \frac{1}{\beta} \sum_{k_y, \omega_n} J_n^{\ell,+}, \quad (\text{S24})$$

$$J_n^{\ell,+} = \frac{iev_y}{2} \left(G_{\ell,21}(x, x, k_y, i\omega_n) - G_{\ell,12}(x, x, k_y, i\omega_n) + G_{\ell,43}(x, x, k_y, i\omega_n) - G_{\ell,34}(x, x, k_y, i\omega_n) \right) - \frac{\ell ev_t}{2} \left(G_{\ell,11}(x, x, k_y, i\omega_n) + G_{\ell,22}(x, x, k_y, i\omega_n) + G_{\ell,33}(x, x, k_y, i\omega_n) + G_{\ell,44}(x, x, k_y, i\omega_n) \right). \quad (\text{S25})$$

With the help of Eq. (S18), one finds

$$J_n^{\ell,+} = \frac{\zeta \ell e \Delta}{\Omega_n} \left(\frac{a_1^\ell e^{-i\ell\theta_1}}{\cos\theta_1} + \frac{a_2^\ell e^{-i\ell\theta_2}}{\cos\theta_2} \right) e^{2\Omega_n x/v_x} + \frac{e|\omega_n|}{\Omega_n} \left(\frac{\zeta_1 b_1 e^{-2ik_1x}}{\cos\theta_1} - \frac{\zeta_2 b_2 e^{2ik_1x}}{\cos\theta_2} \right) + \frac{ie|\omega_n|}{\Omega_n} \sum_{j=1,2} \left(\zeta_j \tan\theta_j + \frac{\ell v_t}{2v_x} \cos\theta_j \right), \quad (\omega_n > 0), \quad (\text{S26})$$

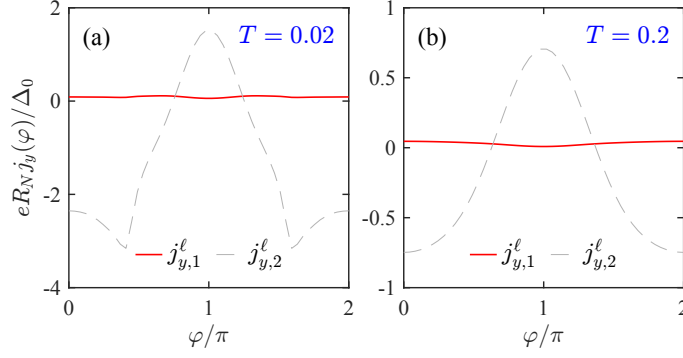


Figure S1. Current-phase relation of $j_y^\ell(\varphi)$ at $\kappa = 1.2$. (a) $T = 0.02$ (in units of T_c). (b) $T = 0.2$.

where $\Omega_n = \sqrt{\omega_n^2 + \Delta^2}$, $\zeta_\ell = (4v_x)^{-1}[ilv_y(1 - e^{i\ell(\theta_1 + \theta_2)}) + lv_t(e^{i\ell\theta_1} + e^{i\ell\theta_2})]$, and $\zeta_{1,2} = (2v_x)^{-1}(v_y + lv_t \sin \theta_{1,2})$. The transverse currents contributed by the Andreev and the normal reflection processes are shown in the first line of Eq. (S26), which are dependent on a^ℓ and b^ℓ , respectively. The mean-field treatment of superconductivity requires the heavy-doping limit in the superconducting regions, *i.e.*, $|\mu_s| \gg \{|\mu|, \Delta\}$ [4, 5]. In this regime we have $\theta_1 \simeq \theta_2 \simeq \theta$ with $\theta = \arctan(v_y k_y / \mu_s)$, and $k_{1(2)} \simeq (\mu_s + (-)\Omega) / v_x$. The frequency component $J_n^{\ell,+}$ contributed by the Andreev processes show exponential decay into the bulk of the superconducting region on the scale of the coherence length $\xi_0 = \hbar v_F / \Delta_0$. However, $J_n^{\ell,+}$ due to the normal reflection are modulated by a rapidly oscillating factor with the length scale $\sim (2\mu_s)^{-1}$, which is much smaller than ξ_0 in the heavy-doping regime. Consequently, the total current contributed by the normal reflection processes is negligible, resulting in

$$J_n^{\ell,+} = \frac{\zeta e \Delta}{2\Omega_n} \left(a_1^\ell(\phi, i|\omega_n|) + a_2^\ell(\phi, i|\omega_n|) \right) e^{2\Omega_n x / v_x} + \frac{i\zeta e |\omega_n|}{\Omega_n}, \quad (\text{S27})$$

$$\zeta = \frac{v_y \tan \theta + lv_t \sec \theta}{v_x}. \quad (\text{S28})$$

For the negative frequency $\omega_n < 0$, the Matsubara Green's function can be obtained by analytic continuation from the advanced Green's function, *i.e.*, $G^A(E - i0^+) \rightarrow G(-i|\omega_n|)$, where the advanced Green's function G^A can be obtained by the similar procedure as we obtain G^R . The transverse current contributed by the negative frequency is given by

$$\langle \hat{j}_y^\ell \rangle_{\omega_n < 0} = \frac{1}{\beta} \sum_{k_y, \omega_n} J_n^{\ell,-}, \quad (\text{S29})$$

$$J_n^{\ell,-} = \frac{\zeta e \Delta}{2\Omega_n} \left(\bar{a}_1^\ell(\phi, -i|\omega_n|) + \bar{a}_2^\ell(\phi, -i|\omega_n|) \right) e^{2\Omega_n x / v_x} - \frac{i\zeta e |\omega_n|}{\Omega_n}. \quad (\text{S30})$$

For a finite $|\omega_n|$, one finds that the imaginary parts of $J_n^{\ell,+}$ and $J_n^{\ell,-}$ are equal in magnitude but opposite in sign, whereas their real parts are the same. Then, the resulting transverse current density is given by

$$\begin{aligned} j_y^\ell &= \langle \hat{j}_y^\ell \rangle_{\omega_n > 0} + \langle \hat{j}_y^\ell \rangle_{\omega_n < 0} = \frac{1}{\beta} \sum_{k_y, \omega_n > 0} \left(J_n^{\ell,+} + J_n^{\ell,-} \right) \\ &= \frac{1}{\beta} \sum_{k_y, \omega_n > 0} \frac{\zeta e \Delta}{\Omega_n} \left(\Re[a_1^\ell(\phi, i\omega_n)] + \Re[a_2^\ell(\phi, i\omega_n)] \right) e^{2\Omega_n x / v_x}. \end{aligned} \quad (\text{S31})$$

We note that the dimensionless coefficient in Eq. (S28) can be rewritten as $\zeta = \zeta_1 + \zeta_2$ with $\zeta_1 = (v_y / v_x) \tan \theta$ and $\zeta_2 = (lv_t / v_x) \sec \theta$, which are related to the direction-dependent velocity v_y and the tilt velocity v_t , respectively. As a result, the transverse current in Eq. (S31) can be decomposed into two parts, *i.e.*, $j_y^\ell = j_{y,1}^\ell + j_{y,2}^\ell$, where $j_{y,1(2)}^\ell = k_B T \sum_{k_y, \omega_n} \zeta_{1(2)} e \Delta / \Omega_n \Re(a_1^\ell + a_2^\ell) e^{2\Omega_n x / v_x}$. In the heavy-doping regime, we have

$$\frac{\zeta_1}{\zeta_2} = \frac{v_y}{v_t} \sin \theta \sim (v_y / v_t) \left| \frac{\mu}{\mu_s} \right| \ll 1, \quad (\text{S32})$$

which results in $j_{y,1}^\ell \ll j_{y,2}^\ell$. The current-phase relation of j_y^ℓ is shown in Figure. S1. It is shown that $j_{y,1}^\ell$ is significantly smaller than $j_{y,2}^\ell$. We note that $j_{y,1}^\ell$ is related to the skew-tunneling and is absent when the scattering is symmetric, i.e., $a_{1,2}^\ell(k_y) = a_{1,2}^\ell(-k_y)$. Whereas $j_{y,2}^\ell$ is attributed to the tilt-induced nonzero transverse momentum acquired by the quasiparticles. Consequently, the predicted transverse Josephson Hall current is dominated by the passage of the Cooper pair across the junction carrying a finite tilt-induced transverse momentum.

* E-mail: zeng@ujs.edu.cn

- [1] W. L. McMillan, Theory of superconductor—normal-metal interfaces, *Phys. Rev.* **175**, 559 (1968).
- [2] Y. Tanaka and S. Kashiwaya, Theory of Josephson effects in anisotropic superconductors, *Phys. Rev. B* **56**, 892 (1997).
- [3] A. Furusaki and M. Tsukada, Dc Josephson effect and Andreev reflection, *Solid State Communications* **78**, 299 (1991).
- [4] C. W. J. Beenakker, Specular Andreev reflection in graphene, *Phys. Rev. Lett.* **97**, 067007 (2006).
- [5] C. W. J. Beenakker, Colloquium: Andreev reflection and Klein tunneling in graphene, *Rev. Mod. Phys.* **80**, 1337 (2008).